Modelling the forced-air cooling mechanisms and performance of polylined horticultural produce

Justin O'Sullivan[1], Maria J. Ferrua[1], Richard Love[1], Pieter Verboven[2], Bart Nicolaï[2], and Andrew East[1]

[1]Massey Institute of Food Science and Technology, Massey University, Private Bag 11-222, Palmerston North 4442, New Zealand, Ph +64 6 350 4336; Fax +64 6 350 5657

[2]University of Leuven, division BIOSYST-MeBioS, Postharvest group, Willem de Croylaan 42, Heverlee, Belgium

Abstract

A 3-D computational fluid dynamics (CFD) model was developed to describe and predict the temperature profiles of palletised polylined kiwifruit packages undergoing forced-air cooling. The geometrical configuration of the kiwifruit, polyliner and cardboard box were explicitly modelled. The model included the effects of natural convection on the airflow behaviour and heat transfer process occurring within the packed fruits inside the polyliner. The capability of the model to predict the fruit temperatures in each package was quantitatively validated against experimental data. A laboratory scaled experimental rig was used to monitor the forced-air cooling process of a half pallet of kiwifruit boxes under controlled operating conditions. The numerical model was able to predict cooling times within experimental error.

Cooling within the pallet was primarily influenced by air temperature and to a lesser extent airflow distribution into each package. A maximum recommend volumetric flowrate through the pallet of 0.34 L kg^{-1} s^{-1}, far lower than flowrates recommended for the cooling of non-

polylined produce, was identified. Successive increases to the flowrate, particularly beyond 0.34 L kg^{-1} s^{-1}, resulted in increasingly diminished reductions (< 12 %) to cooling rate.

Within the polyliner there was a low transfer of energy between kiwifruit and kiwifruit/surrounding air. Instead cooling was reliant on the air temperature flowing over the top of the polyliner.

Keywords: CFD; precooling; horticulture; polyliner; packaging; heat transfer

1. Introduction

Postharvest cooling is essential to ensure that product quality is maintained from harvest to retail. For kiwifruit, the maximum storage potential is achieved when the fruit are cooled to near 0 °C efficiently, shortly after harvest (Ashby, 1995). Kiwifruit, kept at 0 °C and 90 - 95 % relative humidity can have a storage period of 3 to 5 months (Simson & Straus, 2010). This affords market flexibility and eliminates the need for kiwifruit produces to market immediately after harvest. However, improper cooling can lead to hot or cold spots, within the package or pallet, and consequently quality loss in horticulture produce during storage (Verboven et al., 2003). The most common industrial practice to efficiently cool the horticultural produce is a forced-air cooling process immediately after harvest. Forced-air cooling involves forcing refrigerated air through packages of fresh produce stacked upon pallets. Of the different air flow systems available the tunnel cooler is the most common (Brosnan & Sun., 2001).

A variety of factors can affect the cooling times of the produce inside the package. For example, strawberries (a relatively small fruit and packed in individual clamshells within trays) can cool to near 0 °C in as little as 2 h (Ferrua & Singh, 2009c). Conversely, palletized boxes of apples can take up to 12 h to cool (East et al., 2003). Introducing a barrier between the produce and cooling air (as in the case of polylined packaging or fruit wrapped in paper) can extend the cooling period even further. For example, pears stacked in boxes and wrapped in paper can take up to 24 h to cool (Thompson & Chen, 1988).

The typical flowrate range recommended in industry for the forced-air cooling of non-polylined horticultural produce is 0.5 – 2.0 L kg^{-1} s^{-1} (Thompson, 2004). For example, De Castro et al. (2004a) showed that, for the forced-air cooling of non-polylined horticultural produce, increasing the air flowrate from 1 to 2 L kg^{-1} s^{-1} reduced the Half Cooling Time, HCT, by 26 %. For an increase in flowrate from 2 to 4 L s^{-1} kg^{-1} the reduction in HCT was only 11 %.

The packaging structure usually consists of a corrugated cardboard package that contains vents or hand holes to facilitate its handling and provide a means of contact between the refrigerated air and the produce. In addition, depending on the product, individual consumer produces (such as kiwifruit, grapes and berryfruit) are also contained within an internal package. In some situations this is used to separate consumer units of produce, in either bags or clamshells (e.g. strawberries are field packed into individual clamshells, Ferrua & Singh, 2009a). In other cases, including for kiwifruit and grapes (East et al., 2013) a polyliner bag is used to assist in moisture retention of the fruit during the storage period. Following harvest, kiwifruit are at risk of shrivelling if more than 4 % of the total weight at harvest is lost due to water evaporation (Burdon & Lallu, 2011). This affects both its visual appearance and the

selling weight at the end of the supply chain. Kiwifruit are encased within a polyliner to prevent excessive loss of product moisture and maintain product quality.

The growth of computer power in recent years has led to an increased use of numerical models to predict complicated airflow patterns and cooling profiles of horticultural packages during forced-air cooling (Defraeye et al, 2013, 2014; Dehghannya et al., 2008, 2011, 2012; Delele et al., 2008, 2013a, 2013b, 2013c and Ferrua & Singh et al., 2009a, 2009b, 2009c, 2011). The use of numerical modelling facilitates an exact control of different operating conditions, while providing detailed information on the local airflow behaviour and temperature profile within the system. This allows a more fundamental analysis of the design principles and mechanisms underpinning the overall performance of the cooling process.

The aim of this paper was to develop a numerical model to simulate the forced-air cooling of polylined kiwifruit in cardboard packages in a typical industrial pallet layer arrangement used during forced-air tunnel cooling. The model was then used to identify the airflow distribution and temperatures within the pallet and the maximum recommend flowrate, as well as the cooling performance and mechanisms occurring within both the pallet and the polyliner.

2. Materials and methods

2.1 Experimental studies

2.1.1 Industrial forced-air cooling

Hayward kiwifruit (*Actinidia deliciosa*), harvested in Te Puke, New Zealand, are typically packaged in a modular bulk pack (MBP). The MBP consists of a cardboard box with a folding lid at the top, with a 7 cm gap across the middle (Figure 1a). The length, width and depth of the box are 40 cm, 30 cm and 19.5 cm, respectively. Two rectangular vents (hand vents) are located at the top of the front and back face. Hemi-spherical end vents are located at each end face. Inside the box the kiwifruit are contained within a single non-perforated polyliner bag, constructed of high density polyethylene and folded at the top. Each kiwifruit MBP holds approximately 10 kg of kiwifruit, with the exact number of fruit determined by the size grade of the fruit. For this numerical model 100 count 36 kiwifruit, weighing between 93 – 103 g, were contained in each MBP.

A standard ISO industrial pallet (1.2 x 1.0 m) holds 100 MBPs, evenly distributed into 10 layers (Figure 1b). In commercial forced-air cooling operations in New Zealand air is usually pulled through the 1.0 m pallet face (Wilton-Jones, 2012).

2.1.2 Experimental system for validation

A laboratory-scale operation was designed and developed to simulate forced-air cooling of produce stacked a half-pallet high (5 layers, "A" – "E"; Figure 1), while allowing precise control over the temperature and flowrate of the refrigerated air.

For validation purposes a test duct with a solid wooden base, prevented air from been pulled under the pallet (Figure 2). Blocks of insulation where used to fill all the space around the sides of the pallet. This imposed a zero flux condition though the side walls of the pallet. An insulation block was also used to fill the remaining space between the top of the pallet and

125 the fan system. The top and side walls of the test duct were constructed from transparent
126 plastic polycarbonate sheets. A metal duct, containing a wire-mesh at the entrance and exit,
127 was placed in front of the test duct to promote a uniform distribution of the airflow.
128
129 A fan pulled refrigerated air through the pallet in a temperature control room (TCR). A
130 variable speed drive (VSD) was used to fix the flowrate across the pallet. The air flowrate
131 was measured by the pressure drop occurring across an orifice plate located downstream of
132 the palletized structure. For experiments the metal duct containing the wire-mesh, the
133 insulated test duct, the orifice and fan system were all attached together (Figure 2).
134
135 2.1.3 Experimental data collection
136
137 Within the five pallet layers two layers were measured (layers “B” and “D”; Figure 2). Due to
138 the symmetric layout of the pallet layers MBPs 5 and 8, 6 and 9, and 7 and 10, were
139 considered replicas of each other. Hence, only MBPs 1 – 7 were recorded.
140
141 2.1.3.1 Fruit temperature
142
143 In the monitored MBP the kiwifruit were uniformly arranged following a cubic centred
144 distribution pattern. This ensured that airflow distribution and subsequent cooling
145 performance could only be associated with the package design and orientation, and not
146 random stacking of the fruit. A cubic centred distribution could also be replicated in the
147 numerical model.
148

Kiwifruits were separated into four layers within each box. 30 kiwifruit were in the bottom layer, 20 in the second, 30 in the third and 20 in the top. Type-T thermocouples were used to monitor the centre temperatures of 12 kiwifruit within each monitored MBP (Figure 3). Temperatures were logged at one-minute intervals by 64-channel dataloggers (1000 Series Squirrel Meter/Logger, Eltek ltd, Cambridge, UK), over the forced-air cooling periods (approximately 14 h).

2.1.3.2 Air temperature

The air temperature entering the pallet was measured by a thermocouple (1 per vent for the incoming refrigerated airflow into a MBP), giving a total of 4 air measurement points per monitored pallet layer.

2.1.3.3 Experimental conditions

Kiwifruit were stored at 0 °C for approximately 6 weeks following harvest prior to experimentation. Prior to the forced-air cooling experiments the kiwifruit were equilibrated to room temperature (approximately 20 °C), replicating the field heat observed following harvest. The temperature control room was set and maintained at 0 °C, with a relative humidity (RH) of 90 %. On experiment initiation the instrumented pallet was rolled into the room attached to the fan system and the precooling simulation initiated, within 5 minutes of kiwifruit entering the cool environment.

172 Three different flowrates (0.34, 0.51, 0.71 L kg^{-1} s^{-1}) were tested, ranging from low rates
173 (below those for typical precooling operations of non-polylined horticultural produce) to rates
174 within the range (0.5 – 2.0 L kg^{-1} s^{-1}; Thompson, 2004).
175
176 2.2 Model development
177
178 2.2.1 Geometrical configurations
179
180 *Produce arrangement*
181
182 Zespri International provided 2D images of count 36 Hayward kiwifruit (Wilton-Jones,
183 2012). These images gave the dimensions through the centre of the kiwifruit, along the xy-,
184 yz- and xz-axes. The 2D images were converted to Cartesian coordinates and compiled into
185 one representative average 3D geometry of the kiwifruit, in the geometry editor
186 (DesignModeler, 2010).
187
188 The kiwifruit arrangement used in the experimental setup was replicated in the numerical
189 model. Single contact points between individual produce, especially non-spherical produce,
190 can create an unstable and distorted mesh, which can negatively impact the solution accuracy
191 and stability. To promote mesh integrity each individual kiwifruit were kept slightly apart (~
192 2 mm) from each other and the box walls (Figure 3). The bottom layer was the first
193 constructed. 2 mm was found to be the minimum distance that could be used before
194 instabilities began to appear in the numerical simulation. The same distance was maintained
195 between the kiwifruit in the second layer. The arrangement for the bottom and second layer

196 was repeated for the third and top layers. The 100 kiwifruit had a combined surface area and
197 volume of 103.1 x 10^{-2} m^2 and 95.8 x 10^{-4} m^3, respectively (Figure 4a).
198
199 The kiwifruit bulk was encased in a polyliner. The material in the polyliner was high density
200 polyethylene with a thickness of 10 μm. In essence the polyliner is a plastic barrier which
201 wraps around and moulds onto the shape of the external kiwifruit (Figure 4a).
202
203 The polyliner was placed in direct contact with each external kiwifruit by moulding it around
204 the shape of the kiwifruit on the outside of the packed structure, to a depth of 5 mm. A depth
205 < 5 mm introduced computational instabilities (non-converging residuals) to the numerical
206 simulation. Any depth > 5 mm qualitatively appeared to be unrepresentative of reality. Note
207 also that if the polyliner were positioned away from the fruit to avoid contact points, an
208 unrealistic insulating air layer would be created between the polyliner and the fruit, reducing
209 drastically the heat transfer rates across the polyliner. For the implemented case with contact
210 between the polyliner and fruit, a sensitivity analysis (data not included) showed that if the
211 amount of surface area contact increased by 40 % the cooling profiles would change slightly,
212 by initially experiencing faster cooling, but ultimately retain very similar cooling times. The
213 extremely narrow thickness of the polyliner (10 μm) was expected to only provide a physical
214 barrier to airflow but not a thermal barrier to heat transfer. Hence, the polyliner thickness was
215 not included in the numerical model. To reduce the complexity of the mesh the irregular
216 shape of the polyliner was simplified (Figure 4a).
217
218 *Modular bulk pack*
219

220 The cardboard box was constructed with the same dimensions as the physical construct.
221 Some simplification was made to the box, reducing the complex geometry. The
222 hemispherical end vents were replaced with rectangular vents that had the same effective
223 area. The area directly above the end vents created by the gap between the cardboard lids was
224 included in the effective area of the rectangular end vents (Figure 4b).
225
226 When kiwifruit MBPs are stacked in a pallet the refrigerated air that enters through the vents
227 cools not only the kiwifruit in the MBP but also the kiwifruit in MBP directly above, through
228 conduction across the base of the cardboard box (O'Sullivan et al., 2012; 2013). To simulate
229 this phenomenon a periodic boundary condition to link heat transfer from the top of the box
230 to the bottom of the box was required. However, the CFD solver software used (Fluent)
231 cannot simulate a periodic boundary condition between a fluid (air in the gap between the
232 cardboard lid) and a solid (cardboard base). Hence, the two individual cardboard lids were
233 modelled as one lid with the same dimensions as the base of the cardboard box (Figure 4b).
234 The top and bottom of the MBP, both modelled as a continuous solid (cardboard), were
235 linked by the periodic boundary condition in the numerical set-up. The MBP was assembled
236 with the kiwifruit, polyliner and cardboard box (Figure 4b).
237
238 *Pallet footprint*
239
240 The single MBP was multiplied to create a pallet layer. The MBPs were assumed to fit
241 perfectly together with no space between individual packages. Refrigerated air was pulled
242 through the 1.0 m pallet face. To prevent the inlet and outlet boundary conditions from
243 influencing the airflow distribution entering the MBPs, the inlet boundary was located 100
244 cm upstream of the MBP and the outlet boundary 150 cm downstream of the MBP.

245

246 2.2.2 Governing equations

247

248 *Transport phenomenon during forced-air cooling*

249

250 Heat transfer due to conduction and convection were included in the numerical model. For
251 Grashof numbers < 1700 the fluid motions generated by natural convection can be considered
252 negligible (Holdman, 2010). Taking the characteristic dimension as the height of the
253 polyliner (~ 18.3 cm) and a temperature difference of 20 °C (between the refrigerated air and
254 kiwifruit at the start of precooling) the Grashof number was calculated at 2.1 x 10^7,
255 necessitating the inclusion of natural convection in the numerical model.

256

257 Typically, in the forced-air cooling of horticultural produce the influence of radiation is
258 expected to be small compared to the convective heat transfer (Defraeye et al., 2013). During
259 forced-air cooling the heat of respiration is unlikely to have a significant impact on the
260 cooling rate of horticultural produce (Gowda et al., 1997), largely because the forced-air
261 process occurs over a short time period. Additionally, at 10 °C, halfway between initial
262 kiwifruit temperature and temperature of the refrigerated air, that heat of respiration for
263 kiwifruit is relatively low, at 0.37 W (Crisosto et al., 2013). The heat to be removed to cool a
264 single MBP from 20 °C to 0 °C can be calculated from $mC_p\Delta T$. The mass per MBP is 10.5
265 kg, the specific heat capacity of kiwifruit is 3713 J kg^{-1} K^{-1} (Table 1) and the temperature
266 difference is 20 °C. Therefore, the amount if heat to be removed is 780 kJ. Provided the
267 forced-air cooling process does not exceed 29 h to cool a MBP, an unlikely occurrence, then
268 the contribution of the heat of respiration will be < 5 % and can be neglected. Heat transfer

due to moisture loss was experimentally determined to have a negligible impact on the cooling process (data not included).

Transport equations in the numerical model

The momentum transport equations were calculated using the Reynolds-averaged Navier-Stokes equations, described in Versteeg and Malalasekera (1995). The κ-ε turbulence model, with the Enhanced Wall Treatment function enabled, accounted for turbulence in the turbulence regions. Activating gravity, employing the Bousinesq model and defining the volume within the polyliner as a laminar zone in Fluent simulated the effect of natural convection in the polyliner.

Energy transport for fluids

The energy conservation equation was,

$$\frac{\partial}{\partial t}(\rho E) + \nabla \bullet \left(\vec{v}(\rho E + p)\right) = \nabla \bullet \left(k_{eff} \nabla T\right) \quad (1)$$

where E (J kg^{-1}) is the total energy per unit mass, ρ (kg m^{-3}) is the density, p (Pa) is the pressure, v (m s^{-1}) is the velocity, T (°C) is the temperature, t (s) is the time, k_{eff} (W m^{-1} K^{-1}) is the effective thermal conductivity, defined as,

$$k_{eff} = k + k_t \quad (2)$$

where k_t (W m^{-1} K^{-1}) is the turbulent thermal conductivity.

The energy, E, is related to the enthalpy by,

$$E = h - \frac{p}{\rho} + \frac{v^2}{2} \tag{3}$$

h (J kg^{-1}) is the sensible enthalpy,

$$h = \int_{T_{ref}}^{T} C_p dT \tag{4}$$

where C_p (J kg^{-1} K^{-1}) is the heat capacity.

Energy transport for solids

The energy conservation equation in the solid regions (kiwifruit and cardboard) of the numerical model reduced to,

$$\frac{\partial}{\partial t}(\rho h) = \nabla \bullet (k \nabla T) \tag{5}$$

2.2.3 Numerical setup

Thermophysical properties

316 The thermophysical properties of the air and solid materials are defined in Table 1. For
317 temperatures between 0 °C (cooling air temperature) and 20 °C (fruit temperature at the start
318 of forced-air cooling) the thermal properties of air are negligibly affected by temperature and
319 RH (Tsilingiris, 2008). Hence, properties for dry air at 0 °C, found in Holdman (2010), were
320 used for the air. Natural convection was enabled for air inside the polyliner and the air
321 assigned an expansion coefficient.
322
323 The specific heat capacity and thermal conductivity for horticultural produce can be
324 estimated from correlations based on the water content of the produce. The properties for
325 kiwifruit were calculated from the average of series of relevant correlations, found in Sweat
326 (1994). For Hayward kiwifruit harvested in New Zealand the water content (83 %) was
327 calculated from the average of a range of values reported (Macrae et al., 1989; McClone et
328 al., 1998; Mowat and Maguire et al., 2007; Wang et al., 2011) and density from values found
329 in Jordan et al. (2000) and Jordan and Seelye (2009). The thermal properties of corrugated
330 cardboard used in horticultural produce packaging can be found in Tanner (1998; Table 1).
331
332 *Boundary conditions*
333
334 The kiwifruit, polyliner and cardboard surfaces were modelled as no-slip walls with zero
335 roughness. A heat flux of zero was prescribed for side walls of the pallet layer. A periodic
336 boundary condition was enabled between the top and bottom of the MBPs. The temperatures
337 within the computational domain were initially set to the ambient temperature in the
338 laboratory (18.9 – 20.1 °C) where the kiwifruit were equilibrated at prior to validation
339 experiments.
340

Operating conditions

The inlet of the computational domain was defined as a pressure inlet and set to the ambient atmospheric pressure (i.e. the condition in the temperature control room). The outlet of the computational domain was defined as a pressure outlet with an underpressure imposed, to represent the underpressure created by a fan in a forced-air tunnel cooler device. The underpressure was varied to generate the desired flowrate.

For model validation pressure drops of 200, 420 and 850 Pa generated the experimental flowrates of 0.34 L kg^{-1} s^{-1}, 0.51 and 0.71 L kg^{-1} s^{-1}, respectively. To identify an operating condition to recommend pressure drops were doubled from 25 Pa to 800 Pa (i.e. 25, 50, 100, 200, 400 and 800 Pa).

The inlet of the computational domain was set to the temperature of the refrigerated room (~ 0 °C, depending on the specific experimental conditions), while at the outlet a zero gradient of the heat flow was implemented. Low turbulence intensity (1 %) was assumed at the pressure inlet, due to the presence of a screen duct with wire-meshes at the system inlet.

Numerical simulation

The numerical simulations were performed with the ANSYS Fluent 15 software package (Fluent, 2010). The SIMPLE algorithm was used for pressure-velocity coupling. Second order spatial discretization schemes were used throughout.

Computational mesh

366

367 The computational mesh was generated with tetrahedral elements using the ANSYS mesh
368 generation software (Meshing, 2010). The maximum size on any individual face was limited
369 to 7.5 mm. The growth rate or expansion ratio between cells was kept at 1.2, below the
370 maximum of 1.3 recommended in Franke et al. (2007). The total number of elements was 7.4
371 $x10^6$. Richardson extrapolation (Roache, 1997; Franke et al., 2007) was used to estimate the
372 spatial discretization error from the difference in average pallet temperature at the half-
373 cooling time (HCT) with increases to mesh size of 30 %. An error of 1.1 % for a mesh size of
374 7.4 $x10^6$ elements was considered sufficiently low.

375

376 Iterative convergence

377

378 To reduce the total computational time the flow field was initialized by solving the
379 momentum equations at steady-state and independent of temperature. The transient
380 simulation was run, with the energy and momentum equations coupled together to account
381 for the effect of natural convection. The exclusion of natural convection, and the subsequent
382 velocity field, caused the numerical model to predict HCTs up to 21.9 % slower than when
383 natural convection was simulated, necessitating the inclusion of natural convection (data not
384 shown). The transient simulation was run at a time step of 60 s, with a maximum of 20
385 iterations per time step. A temporal analysis on the time step size was performed, with
386 Richardson extrapolation (Roache, 1997) for the average pallet temperature at HCT. Relative
387 errors were 0.3 %, 1.0 % and 3.1 % for times steps of 15 s, 30 s and 60 s, respectively (data
388 not shown). A time step of 30 s extended the simulation time more than two fold, making 60
389 s an acceptable compromise between solution accuracy and computation time. The flow and
390 turbulence equations were calculated along with the energy equation during transient

391 simulation. The simulations (for 14 h) took approximately 24 h, on an i5-4570 Intel Core
392 processor (3.2 GHz) with 8 GB RAM memory.
393
394 2.3 Data Analysis – model validation
395
396 Numerical model validation consisted of comparing numerical and experimental half-cooling
397 times (HCT) and seven-eighths cooling times (SECT) for individual MBPs within a pallet
398 layer.
399
400 To calculate the cooling times the kiwifruit temperatures were first converted to the fractional
401 unaccomplished temperature change (FUTC), *Y*. *Y* represents the amount of possible
402 temperature change that has yet to be accomplished (Eq. 6) and is a common method used to
403 normalise cooling data (Brosnan and Sun, 2001).
404
405 $$Y = \frac{T - T_a}{T_i - T_a} \quad (6)$$
406
407 where T (°C) is the temperature of kiwifruit in MBP at the specified time of cooling, T_i (°C)
408 is the initial temperature of individual kiwifruit in the MBP at the start of cooling, and T_a (°C)
409 is the average temperature of the air. T_a (°C) is a single value, taken as the average
410 temperature of the air entering the pallet over the cooling process. When calculating the
411 averaging *Y* during experiments in a MBP *Y* was first calculated for each kiwifruit and then
412 averaged over the number of kiwifruit recorded per MBP. The HCT is defined as the time at
413 where Y equals 0.5, when the kiwifruit has cooled halfway from their initial temperature to
414 that of the cooling air. The SECT is when Y = 0.125.
415

3. Results

3.1 Cooling mechanisms and performance

3.1.1 Cooling within the pallet layer

The airflow distribution within each MBP caused relatively high air velocities immediately behind the inlet vents of each MBP that quickly dissipated within the MBPs (Figure 5a).

MBPs 1 and 5, located at the front of the pallet and directly exposed to the incoming refrigerated air, had the shortest HCTs (Table 2). Over half the airflow entering the front of the pallet flowed into MBP 1, located in the centre (Figure 5b). The remaining 44.0 % was split evenly between MBPs 5 and 8, located at the side of the pallet. The airflow was pulled from the front to the back of the pallet with only a small exchange of airflow (< 3.2 %) between MBPs located along the centre and side of the pallet.

The rise in temperature of the cooling air as it was pulled through the pallet (Figure 6) resulted in slower cooling rates for the MBPs at the back of the pallet (MBPs 3, 4, 6 and 7), where the airflow distributed a higher percent through the centre of the pallet, causing lower air temperatures and faster cooling in the corresponding MBPs (i.e. the HCT of MBP 3 < MBP 6 and the HCT of MBP 4 < MBP 7, despite their longer distances from the front of the pallet; Table 2).

Differences in the HCT of individual MBPs result from changes to the air flowrate and/or the temperature difference between the cooling air and the polyliner. Reductions in HCT of

441 MBPs 1 and 5 are largely associated with an increase in air flowrate as the air temperature
442 entering the MBPs was effectively constant, due to the MBP location at the front of the pallet
443 (Figure 6). The HCT for MBPs 1 and 5 were at an effective maximum (< 12 % reduction in
444 HCT for each successive pressure drop increase; Table 2). This suggests that the
445 comparatively larger reductions in HCT for MBPs 3, 4, 6 and 7 were largely associated with
446 a lower increment of air temperature along the pallet (Figure 6) rather than increases to air
447 flowrate.
448
449 The efficiency of the forced-air cooling process is determined by the rate and uniformity of
450 product cooling in comparison to the energy input required (de Castro et al., 2004a, 2004b).
451 The power requirement, W (W), is a product of the flowrate and pressure drop. Successive
452 increases to the pressure drop after 200 Pa (0.34 L kg^{-1} s^{-1}) result in relative reductions to the
453 average pallet layer HCT < 12 % (Table 2). The extra power requirements, coupled with the
454 diminishing reduction in improvement to HCT, make substantial increases of pressure drop
455 an inefficient method of improving the forced air cooling process of polylined horticultural
456 produce. Hence, pressure drops beyond 200 Pa (0.34 L kg^{-1} s^{-1}) are not recommended for use
457 in industry, particularly when the associated operating costs to run the fan to generate the
458 pressure drops are taken into consideration.
459
460 3.1.2 Cooling profiles within MBPs
461
462 Temperature distribution images were generated at a flowrate of 0.34 L kg^{-1} s^{-1} (200 Pa),
463 from an initial temperature of 20 °C, after 4.28 h of forced-air cooling, the average pallet
464 layer HCT (Figure 7).
465

466 The airflow through the pallet brought refrigerated air into contact with the polyliner. The
467 kiwifruit in contact with the polyliner (i.e. kiwifruit at the top and sides of the fruit bulk) had
468 relatively low surface temperatures (Figure 7). The periodic boundary condition, simulating
469 the heat transfer pathway provided by refrigerated airflow entering pallet layer stacked
470 directly below, caused relatively rapid cooling in the bottom kiwifruit layer, similar to the
471 cooling in the top layer. With only the heat transfer mechanisms of natural convection and
472 effective conduction with the adjoining kiwifruit present, kiwifruit in the centre of the MBP
473 cooled relatively slowly. This created large temperature gradients between the centre and
474 edge kiwifruit, within each MBP.
475
476 The kiwifruit in the centre of the bulk, with no contact with the refrigerated airflow limited
477 the impact of increasing the flowrate through the pallet. For polylined produce the polyliner
478 prevented direct contact between the refrigerated air and the produce. The polyliner, which
479 moulded to the shape of the external fruit bulk, created a much smaller surface area for the air
480 to contact than the potential surface area if the refrigerated air flowed between and around
481 each individual product. With a lower surface area for contact between refrigerated air and
482 produce (or polyliner in this case) a lower volumetric flowrate (0.34 L kg^{-1} s^{-1}), than typically
483 recommended for non-polylined produce (0.5 – 2.0 L kg^{-1} s^{-1}; Thompson, 2004), was
484 required to reach the recommend maximum flowrate, beyond which relatively small
485 improvements to cooling time for drastically increasing power requirements were observed.
486
487 3.2 Experimental validation
488
489 Validation of the numerical model was achieved by examining the computed and
490 experimental cooling profiles (Figure 8) and HCT and SECT for each MBP at each of the

491 tested flowrates (Figure 9). The experimental uncertainty (standard error) was calculated per
492 MBP. The experimental average temperature was calculated by averaging the 12 data points
493 recorded in each MBP. The standard error was calculated from 24 data points (12 per MBP in
494 each of the two monitored layers) for MBP 1 – 4 and from 48 data points for MBP 5 – 7.
495
496 3.2.1 Comparison of the computed and experimental temperature profiles
497
498 Separating the pallet layer into MBPs 1 – 4 (through the centre of the pallet layer) and MBPs
499 5 – 7 (along the side of the pallet layer), with error bars only presented for MBPs 1, 4, 5 and
500 7, allowed for a more detailed comparison of the individual MBP temperature profiles
501 (Figure 8).
502
503 The predicted temperature profiles fell within the standard error bars of the experimental data
504 (Figure 8). While the predicted temperatures remained within the error bars for the duration
505 of the simulation they tended to over predict the temperate drop at the start of cooling (0 – 4
506 h) and under predict the kiwifruit temperatures at end of the cooling operation (12 – 14 h).
507 Overall, the location of the predicted temperature profiles, within the error bars of the
508 experimental data, showed the goodness of fit of the CFD model.
509
510 With the exception of the SECT for MBP 6 and 7 at a flowrate of 0.51 L kg^{-1} s^{-1} the HCT and
511 SECT predicted by the numerical model fall within the error bars of the experiments for each
512 of the tested flowrates (Figure 9).
513
514 While minor, the discrepancies observed between experimental and predicted data could be
515 the result of a wide range of factors. The slight over prediction of cooling (i.e. kiwifruit

516 temperatures were predicted lower than experimental values) at the start of the simulations
517 (Figures 8 and 9) can most likely be explained by the exact thermocouple location. During
518 experiments the thermocouples were placed as close to the centre of the kiwifruit as possible
519 (i.e. the slowest cooling point within the fruit). However, the numerical model monitors the
520 average temperature of the entire kiwifruit volume (including those lower temperatures that
521 immediately start developing close to the fruit surface).
522
523 In experiments the wires may have caused some blockage of the vents in the MBPs. A
524 blockage would have a greater impact on MBPs 5 – 7 due to the smaller vent area orientated
525 perpendicular to the incoming refrigerated airflow (13 cm^2 compared to 44 cm^2 for MBPs 1 –
526 4).
527
528 Other factors include the complexity of the transport phenomenon modelled, uncertainties in
529 material properties (i.e. specific heat capacity and thermal conductivity of the kiwifruit) and
530 differences in the shape and size of the fruit and the influence of the intrusive temperature
531 measurement technique on the flow field. However, only small differences were observed
532 between experimental and numerical values, proving the viability of the developed model,
533 especially when considering the large mass of fruit per MBP (~10 kg) and long duration (14
534 h) of the forced-air cooling operations.
535
536 4. Conclusions
537
538 A numerical model to simulate the forced-air cooling for a single pallet layer containing 10
539 polylined kiwifruit MBPs has been developed and validated. The polyliner created an
540 enclosed space, consisting of air and the produce where the primary methods of heat transfer

were natural convection and conduction. Hence the effect of natural convection must be simulated when dealing with horticultural produce encased in a polyliner.

Unlike the cooling of produce without a polyliner there was no direct contact between refrigerated airflow and produce. As a result the conductive cooling through the base of the cardboard box, supplied by the airflow pulled through the MBP directly beneath has a greater influence on the overall heat transfer rate and must be included in the numerical model. Hence, a periodic boundary condition linking heat transfer between the top and bottom of the MBPs was included to simulate the cooling effect of the airflow entering MBPs in the pallet layers directly below the simulated layer.

The capability of the numerical model to predict the average fruit temperature per MBP was quantitatively validated. A good agreement was found between the experimental and predicted temperature profiles and the values of HCT and SECT for each MBP. Considering the complexity of the transport phenomena controlling the cooling performance of the process the level of agreement found between experimental and predicted data confirmed the goodness of fit of the developed model.

The numerical model can be used to predict the transport phenomenon within the individual MBPs during forced-air cooling applications and provide insight into the heat transfer mechanisms occurring within the polyliner. With no forced-convective cooling mechanisms within the polyliner fruit in the centre of the MBP cool relatively slowly compared to fruit in direct contact with the polyliner or cardboard base.

Cooling of individual MBPs was influenced by air flowrate, distance from incoming refrigerated airflow, airflow distribution into each MBP, package orientation and air temperature into each MBP. The reduced impact of air flowrate, compared to the forced-air cooling of non-polylined horticultural produce, results in a relatively low maximum recommend flowrate, above which the impact of increasing the flowrate has a diminished impact on the cooling rate of the polylined produce.

The numerical model can now be used to assess a variety of operating conditions and evaluate the results in terms of cooling rate, uniformity, energy cost and pallet throughput per week. The results of these numerical studies can be used to determine an optimal operating point that can promote relatively rapid cooling of the produce, without incurring excessive operational costs.

Additionally, alternative packages can be designed and their impact on cooling performance numerically assessed. Alternative packages can focus on improving cooling uniformity or pallet throughput per week, depending on the requirements of the industrial operator.

Acknowledgements

This paper is an output of the PhD research of Justin O'Sullivan as supported by a Zespri™ International PhD scholarship and the Ministry of Business, Employment and Innovation funded Fibreboard Packaging Design research project (MAUX 1302).

590

591

592 References
593

594 Ashby, B.H. (1995). Protecting perishable foods during transport by truck. *Handbook no. 669.* USDA.
595 Washington, D.C.

596 ASHRAE. (1993). *ASHRAE handbook: Fundamentals*. Atlanta, GA: American Society of
597 Heating, Refrigeration and Air-Conditioning Engineers.

598 Brosnan, T., & Sun, D-W. (2001). Precooling techniques and applications for horticultural products –
599 a review. *International Journal of Refrigeration*, 24(2), 154-170.
600 doi:10.1016/S0140-7007(00)00017-7

601 Burdon, J., & Lallu, N. (2011). Kiwifruit (Actinidia spp.). In: E.M. Yahia (Ed.), *Postharvest biology*
602 *and technology of tropical and subtropical fruits. Volume 3: coconut to mango* (pp. 326-360).
603 Woodhead Publishing Limited, Cambridge, UK.

604 Crisosto, C.H., Mitcham, E.J., & Kader, A.A. (2013). *Kiwifruit: recommendations for maintaining*
605 *postharvest quality.* Retrieved from http://postharvest.ucdavis.edu/PFfruits/Kiwifruit/

606 de Castro, L.R., Vigneault, C., & Cortez, L.A.B. (2004a). Effect of container opening area on air
607 distribution during precooling of horticultural produce. *Transactions of ASAE*, 47(6), 2033–2038.
608 doi:10.13031/2013.17792

609 de Castro, L.R., Vigneault, C., & Cortez, L.A.B. (2004b). Container opening design for horticultural
610 produce cooling efficiency. *Food, Agriculture and Environment*, 2(1), 135–140.

611 Defraeye, T., Lambrecht, R., Tsige, A.A, Delele, M.A., Opara, U.L., Cronjé, P., Verboven, P., &
612 Nicolaï, B.M. (2013). Forced-convective cooling of citrus fruit: package design, *Journal of Food*
613 *Engineering,* 118(1), 8-18. doi:10.1016/j.jfoodeng.2013.03.026

614 Defraeye, T., Lambrecht, R., Delele, M.A., Tsige, A.A, Opara, U.L., Cronjé, P., Verboven, P., &
615 Nicolaï, B.M. (2014). Forced-convective cooling of citrus fruit: cooling conditions and energy
616 consumption in relation to package design, *Journal of Food Engineering,* 121, 118-127.
617 doi:10.1016/j.jfoodeng.2013.08.021

618 Dehghannya, J.M., Ngadi, M., & Vigneault, C. (2008). Simultaneous aerodynamic and thermal
619 analysis during cooling of stacked spheres inside ventilated packages, *Chemical Engineering &*
620 *Technology,* 31(11), 1651-1659. doi:10.1002/ceat.200800290

621 Dehghannya, J.M., Ngadi, M., & Vigneault, C. (2011). Mathematical modeling of airflow and heat
622 transfer during forced convection cooling of produce considering various package vent areas, *Food*
623 *Control,* 22(8), 1393-1399. doi:10.1016/j.foodcont.2011.02.019

624 Dehghannya, J.M., Ngadi, M., & Vigneault, C. (2012). Transport phenomena modelling during
625 produce cooling for optimal package design: Thermal sensitivity analysis, *Biosystems Engineering,*
626 111(3), 315-324. doi:10.1016/j.biosystemseng.2012.01.001

627 Delele, M.A., Tijskens, E., Atalay, Y., Ho, Q., Ramon, H., Nicolaï, B.M., & Verboven, P. (2008).
628 Combined discrete element and CFD modelling of airflow through random stacking of horticultural
629 products in vented boxes, *Journal of Food Engineering,* 89(1), 33-41.
630 doi:10.1016/j.jfoodeng.2008.03.026

631

632 Delele, M.A, Ngcobo, M.E.K., Opara, U.L., & Meyer, C.J. (2013a). Investigating the Effects of Table
633 Grape Package Components and Stacking on Airflow, Heat and Mass Transfer Using 3-D CFD
634 Modelling. *Food and Bioprocess Technology*, 6(9), 2571-2585. doi:10.1007/s11947-012-0895-5

635 Delele, M.A, Ngcobo, M.E.K., Getahun, S.T., Chen, L., Mellmann, J., & Opara, U.L. (2013b).
636 Studying airflow and heat transfer characteristics of horticultural produce packaging system using 3-D
637 CFD model. Part I: Model development and validation. *Postharvest Biology and Technology,* 86, 536-
638 545. doi:10.1016/j.postharvbio.2013.08.014

639 Delele, M.A, Ngcobo, M.E.K., Getahun, S.T., Chen, L., Mellmann, J., & Opara, U.L. (2013c).
640 Studying airflow and heat transfer characteristics of a horticultural produce packaging system using 3-
641 D CFD model. Part II: Effect of package design. *Postharvest Biology and Technology,* 86, 546-555.
642 doi:10.1016/j.postharvbio.2013.08.015

643 DesignModeler. (2010). Canonsburg, PA: Ansys Inc.

644 East, A.R., Sabarez, H.T., Tanner, D.J., & Cleland, D.J. (2003). Validation of a Packaging Design
645 Tool: Case Study for Appple Packaging, *Proc. International Congress of Refrigeration*, Washington,
646 D.C

647 East, A.R., Jeffery, P.B., & Love, R.J. (2013) Investigating asymmetrical packaging as a technique to
648 reduce heterogeneity during pre-cooling of fresh produce, *Proc. 2nd IIR International Conference on*
649 *Sustainability and the Cold Chain,* Paris, France.

650 Ferrua, M.J., & Singh, R.P. (2009a). Modeling the forced-air cooling process of fresh strawberry
651 packages, Part I: Numerical model, *International Journal of Refrigeration,* 32(2), 335-348.
652 doi:10.1016/j.ijrefrig.2008.04.010

653 Ferrua, M.J., & Singh, R.P. (2009b). Modeling the forced-air cooling process of fresh strawberry
654 packages, Part II: Experimental validation of the flow model, *International Journal of Refrigeration,*
655 32(2), 349-358. doi:10.1016/j.ijrefrig.2008.04.009

656 Ferrua, M.J., & Singh, R.P. (2009c). Modeling the forced-air cooling process of fresh strawberry
657 packages, Part III: Experimental validation of the energy model, *International Journal of*
658 *Refrigeration,* 32(2), 359-368. doi:10.1016/j.ijrefrig.2008.04.011

659 Ferrua, M.J., & Singh, R.P. (2011). Improved airflow method and packaging system for forced-air
660 coolnig of strawberry packaging, *International Journal of Refrigeration,* 34(4), 1162-1173.
661 doi:10.1016/j.ijrefrig.2011.01.018

662 Fluent. (2010). Canonsburg, PA: Ansys Inc.

663 Fluent-Theory. (2010). Canonsburg, PA: Ansys Inc.

664 Franke, J., Hellsten, A., Schlünzen, H., & Carissimo, B. (2007) *Best practice guideline for CFD*
665 *simulation of flows in the urban environment. COST Action 732: Quality Assurance and Improvement*
666 *of Microscale Meteorological Models.* University of Hamburg, Hamburg, Germany.

667 Gowda, B.S., Narasimham, G.S.V.L., & Murthy, M.V.K. (1997). Forced-air precooling of spherical
668 foods in bulk: A parametric study. *International Journal of Heat and Fluid Flow*, 18(6), 613-624.
669 doi:10.1016/S0142-727X(97)00028-3

670 Holman, J.P. (2010). *Heat Transfer* (10th ed.). McGraw-Hill, New York, NY.

671 Jordan, R.B., Walton, E.F., Klages, K.U., & Seelye, R.J. (2000). Postharvest fruit density as an
672 indicator of dry matter and ripened soluble solids of kiwifruit, *Postharvest Biology and Technology*,
673 20(2), 163-173. doi:10.1016/S0925-5214(00)00125-3

674 Jordan, R.B., & Seelye, R.J. (2009) Relationship between taste perception, density and soluble solids
675 concentration in kiwifruit (Actinidia deliciosa), *New Zealand Journal of Crop and Horticultural*
676 *Science*, 37(4), 303-317. doi:10.1080/01140671.2009.9687585

677 Macrae, E. A., Bowen, J.H., & Margaret, G.H.S. (1989). Maturation of kiwifruit (Actinidia deliciosa
678 cv Hayward) from two orchards: Differences in composition of the tissue zones, *Journal of the*
679 *Science of Food and Agriculture,* 47(4), 401-416. doi:10.1002/jsfa.2740470403

680 McGlone, V.A., & Kawano, S. (1998). Firmness, dry-matter and soluble-solids assessment of
681 postharvest kiwifruit by NIR spectroscopy, *Postharvest Biology and Technology,* 13(2), 131-141.
682 doi:10.1016/S0925-5214(98)00007-6

683 Meshing. (2010). Canonsburg, PA: Ansys Inc.

684 Mowat, A., & Maguire, K. (2007). Canopy management and dry matter of 'Hayward' kiwifruit. *Acta*
685 *Hortic,* 753, 333-340. doi:10.17660/ActaHortic.2007.753.41

686 O'Sullivan, J.L., Ferrua, M., Love, R., Verboven, P., Nicolai, B.M., & East, A. (2012).
687 Mechanisms and performance of the forced-air cooling process of fruit packed in
688 polyethylene liners, *CIGR Section VII International Technical Symposium on Innovating the*
689 *Food Value Chain,* Stellenbosch, South Africa.

690 O'Sullivan, J.L., Ferrua, M.J., Love, R.J., Verboven, P., Nicolaï, B.M., & East, A.R. (2013a)
691 Performance of the forced-air cooling process of fruit packed in polyethylene liners as a function of
692 pallet orientation, *Proc. 2nd IIR International Conference on Sustainability and the Cold Chain,* Paris,
693 France.

694 O'Sullivan, J.L., Ferrua, M.J., Love, R.J., Verboven, P., Nicolaï, B.M., & East, A.R. (2014). Airflow
695 measurement techniques for the improvement of forced-air cooling, refrigeration and drying
696 operations, *Journal of Food Engineering,* 143, 90-101. doi:10.1016/j.jfoodeng.2014.06.041

697 Roache, P.J. (1997). Quantification of uncertaintity in compuational fluid dynamics. *Annual reviw of*
698 *Fluid Mechanics*, 29, 123-160. doi:10.146/annurev.fluid.29.1.123

699 Simson, S. P., & Straus, M.C. (2010). Post-Harvest Technolgy of Horticulture Crops. Oxford Book
700 Company, New Delhi, India

701 Sweat, V.E. (1994). Thermal properties of food. In M.A. Rao & S.S.H. Rizvi (Eds.), *Engineering*
702 *properties of foods* (2nd ed., pp. 99-138). Marcel Dekker, Inc., New York, NY.

703 Tanner, D.J. (1998*). Mathematical modelling for design of horticultural packaging* (Doctoral
704 dissertation, Massey University, Palmerston North, New Zealand). Retrieved from
705 http://hdl.handle.net/10179/2824

706 Thompson, J., & Chen, Y. (1988). Comparative energy use of vacuum, hydro, and forced air coolers
707 for fruits and vegetables. *ASHRAE Transactions*, 92, 1427-1433. Retreived from
708 http://ucanr.edu/datastoreFiles/234-1044.PDF

709 Thompson, J. (2004). Pre-Cooling and Storage Facilities. In USDA (Ed.), *USDA Agriculture*
710 *Handbook 66: The Commercial Storage of Fruits, Vegetables, and Florist and Nursery Stocks* (pp. 1-
711 10). USDA, Washington, DC.

712 Tsilingiris, P.T. (2008). Thermophysical and transport properties of humid air at temperature range
713 between 0 and 100 °C, *Energy Conversion and Management*, 49(5), 1098-1110.
714 doi:10.1016/j.enconman.2007.09.015

715 van der Sman, R.G.M. (2002). Prediction of airflow through a vented tray by the Darcy–Forchheimer
716 equation. *Journal of Food Engineering,* 55(1), 49-57. doi:10.1016/S0260-8774(01)00241-2

717 Verboven, P., Hoang, M.L., & Nicolaï, B.M. (2003). Modelling turbulent air flow in cool rooms for
718 horticultural products. *Acta Hortic,* 599, 435-441. doi:10.17660/ActaHortic.2003.599.55

719 Versteeg, H.K., & Malalasekera, W. (1995). *An introduction to computational fluid dynamics: the*
720 *finite volume method*. Essex, England: Longman Scientific & Technical.

721 Wang, M.Y., MacRae, E. Wohlers, M., & Marsh, K. (2011). Changes in volatile production and
722 sensory quality of kiwifruit during fruit maturation in Actinidia deliciosa 'Hayward' and A. chinensis
723 'Hort16A', *Postharvest Biology and Technology,* 59(1) 16-24. doi:10.1016/j.postharvbio.2010.08.010

724 Wilton-Jones, S. (2012). Personal Communication, Zespri International Ltd, Mt Maunganui, New
725 Zealand.

726

Highlights

- CFD model of the forced-air cooling process of polylined horticultural produce
- Validated model of a complete pallet layer (10 kiwifruit packages)
- Cooling mechanisms both inside and outside the polyliner modelled
- Cooling influenced by air temperature and distribution within pallet layer
- Little cooling rate benefit to increasing flowrate beyond 0.34 L kg^{-1} s^{-1}

Figures

Figure 8. Comparison between predicted and experimental numerical average temperatures, during 14 h of forced-air cooling from an approximate initial product temperature of 20 °C, for (a) MBPs 1 - 4 at 0.34 L kg^{-1} s^{-1}, (b) MBPs 5 - 7 at 0.34 L kg^{-1} s^{-1}, (c) MBPs 1 - 4 at 0.51 L kg^{-1} s^{-1}, (d) MBPs 5 - 7 at 0.51 L kg^{-1} s^{-1}, (e) MBPs 1 - 4 at 0.71 L kg^{-1} s^{-1} and (f) MBPs 5 - 7 at 0.71 L kg^{-1} s^{-1}. Standard error bars are shown for MBPs 1, 4, 5 and 7. Experimental and predicted air temperatures, averaged between the inlet vents of MBPs 1 and 5, are also shown.

Figure 9. Predicted and experimental cooling times for MBPs 1 – 7 for (a) HCT at 0.34 L kg^{-1} s^{-1}, (b) SECT at 0.34 L kg^{-1} s^{-1}, (c) HCT at 0.51 L kg^{-1} s^{-1}, (d) SECT at 0.51 L kg^{-1} s^{-1}, (e) HCT at 0.71 L kg^{-1} s^{-1} and (f) SECT at 0.71 L kg^{-1} s^{-1}. Standard error bars are shown for each MBP.

Figure 1

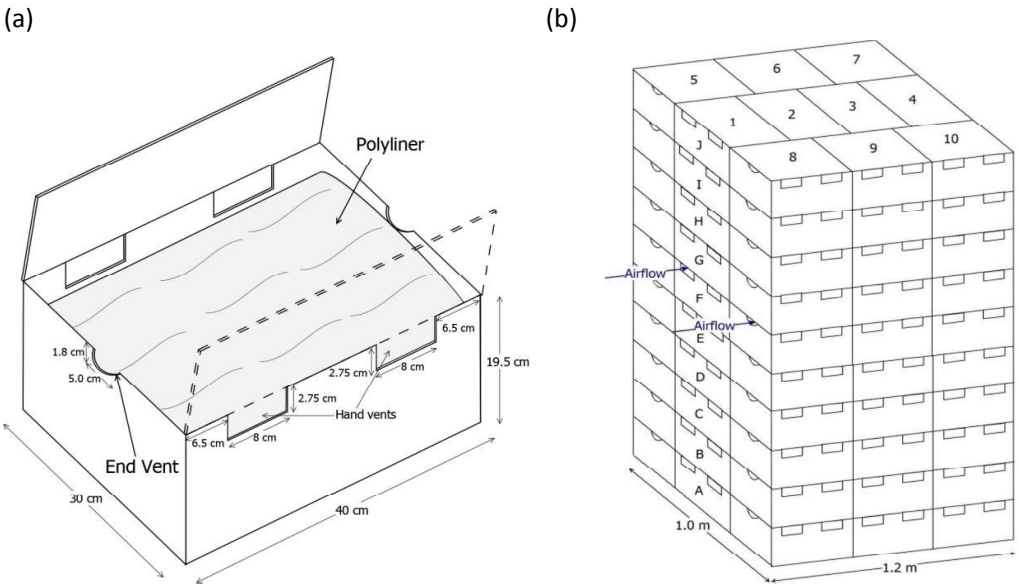

Figure 1. (a) Modular bulk pack (MBP) for Hayward green kiwifruit and (b) palletised kiwifruit in MBPs numbered 1 – 10 and pallet layers “A” – “J”. Air is drawn through the 1.0 m face.

Figure 2

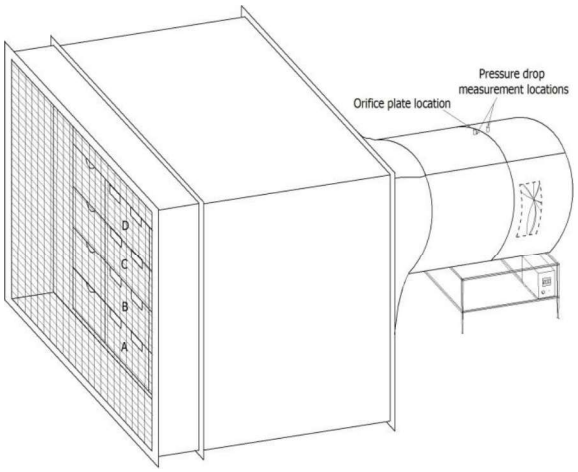

Figure 2. Half-pallet layout with wire mesh and insulated test duct attachments for the forced-air cooling system.

Figure 3

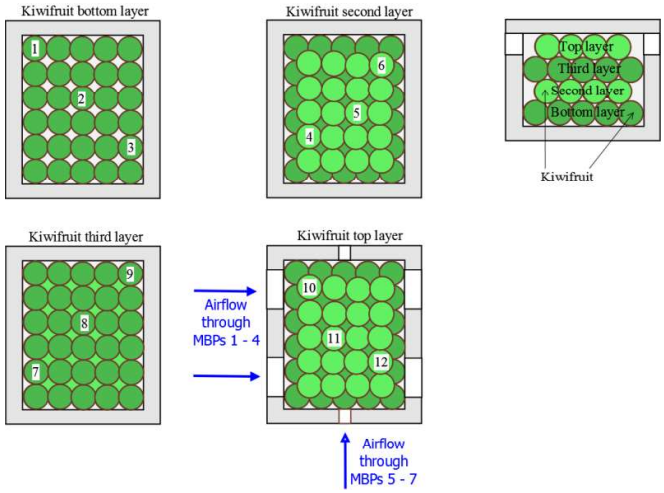

Figure 3. Cubic centred distribution and thermocouple location for kiwifruit in the MBPs

Figure 4

(a) (b)

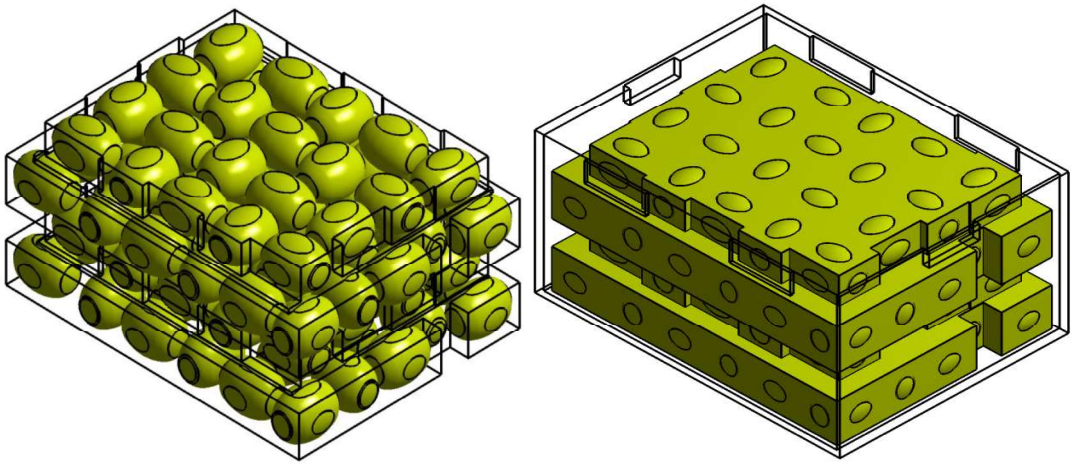

Figure 4. Image of (a) effective polyliner surface and kiwifruit bulk and (b) complete MBP.

Figure 5

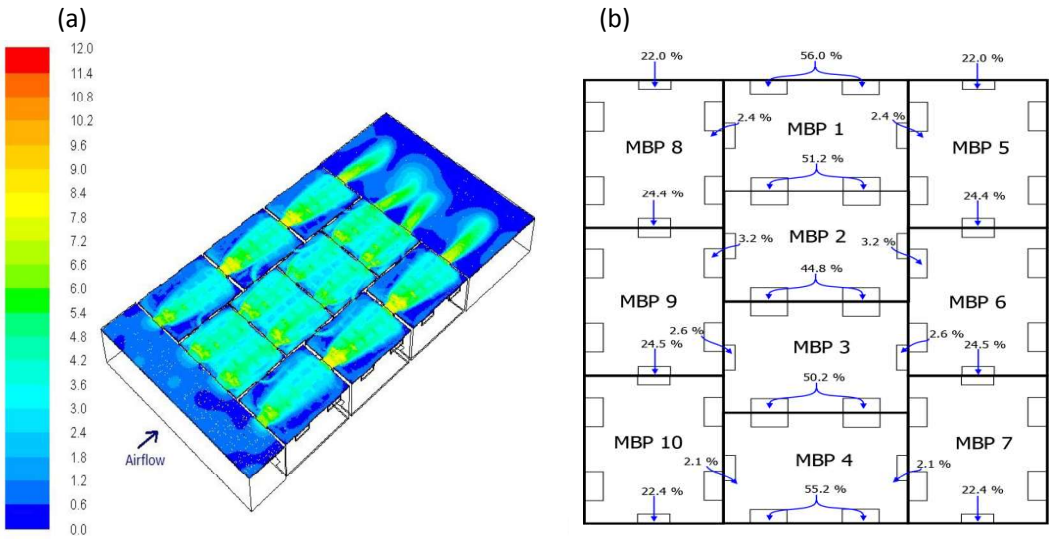

Figure 5. Distribution of (a) air velocity (m s^{-1}) and (b) flowrate (%) between MBPs (total entering and exiting the pallet layer of 100 %) for a pressure drop of 200 Pa (0.34 L kg^{-1} s^{-1}). Arrows denotes net airflow transfer direction.

Figure 6

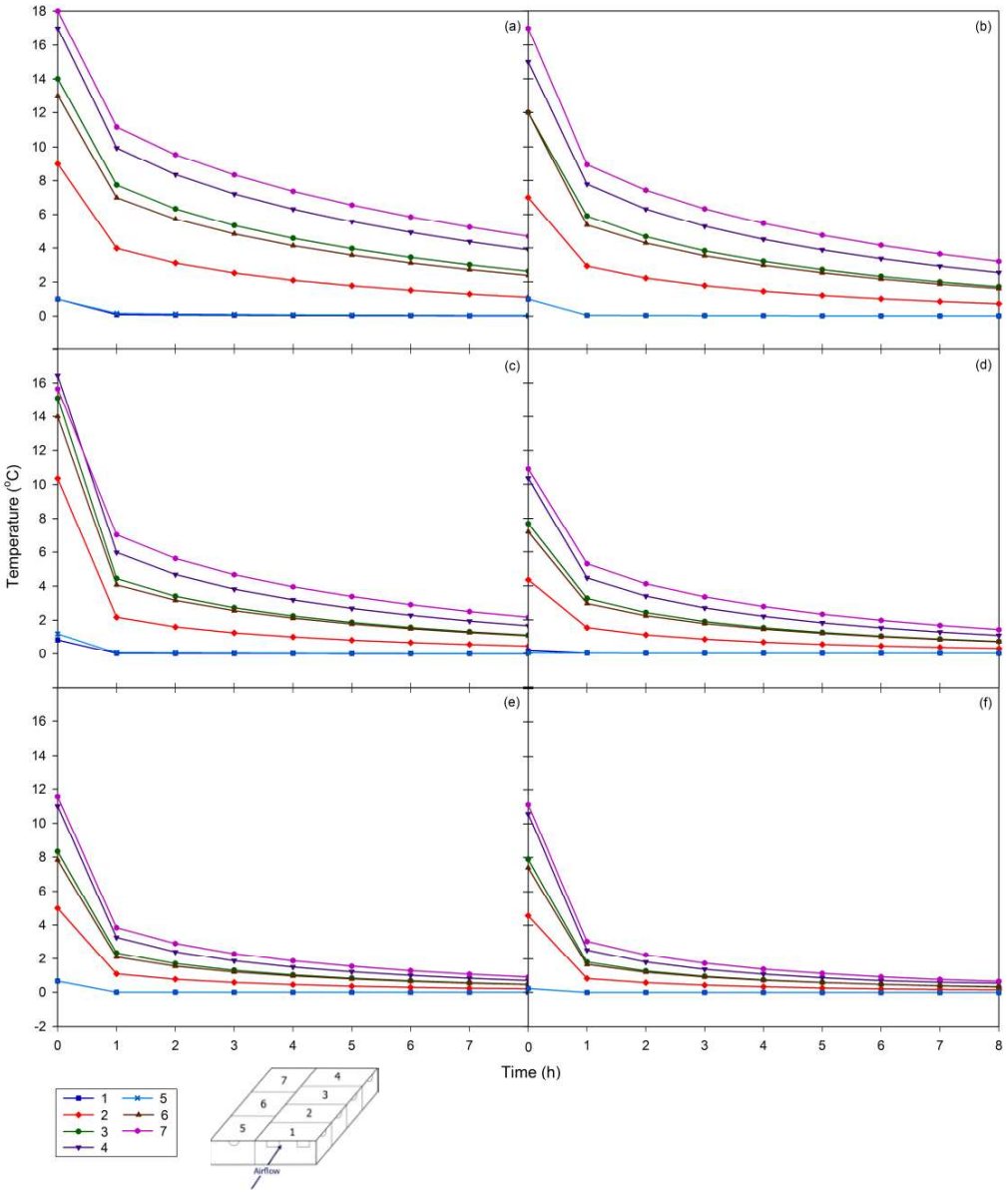

Figure 6. Average air temperature at the inlet vents (perpendicular to the incoming refrigerated air pulled through the pallet layer) for MBPs 1 – 7 at pressure drops of (a) 25 Pa, (b) 50 Pa, (c) 100 Pa, (d) 200 Pa, (e) 400 Pa and (d) 800 Pa.

Figure 7

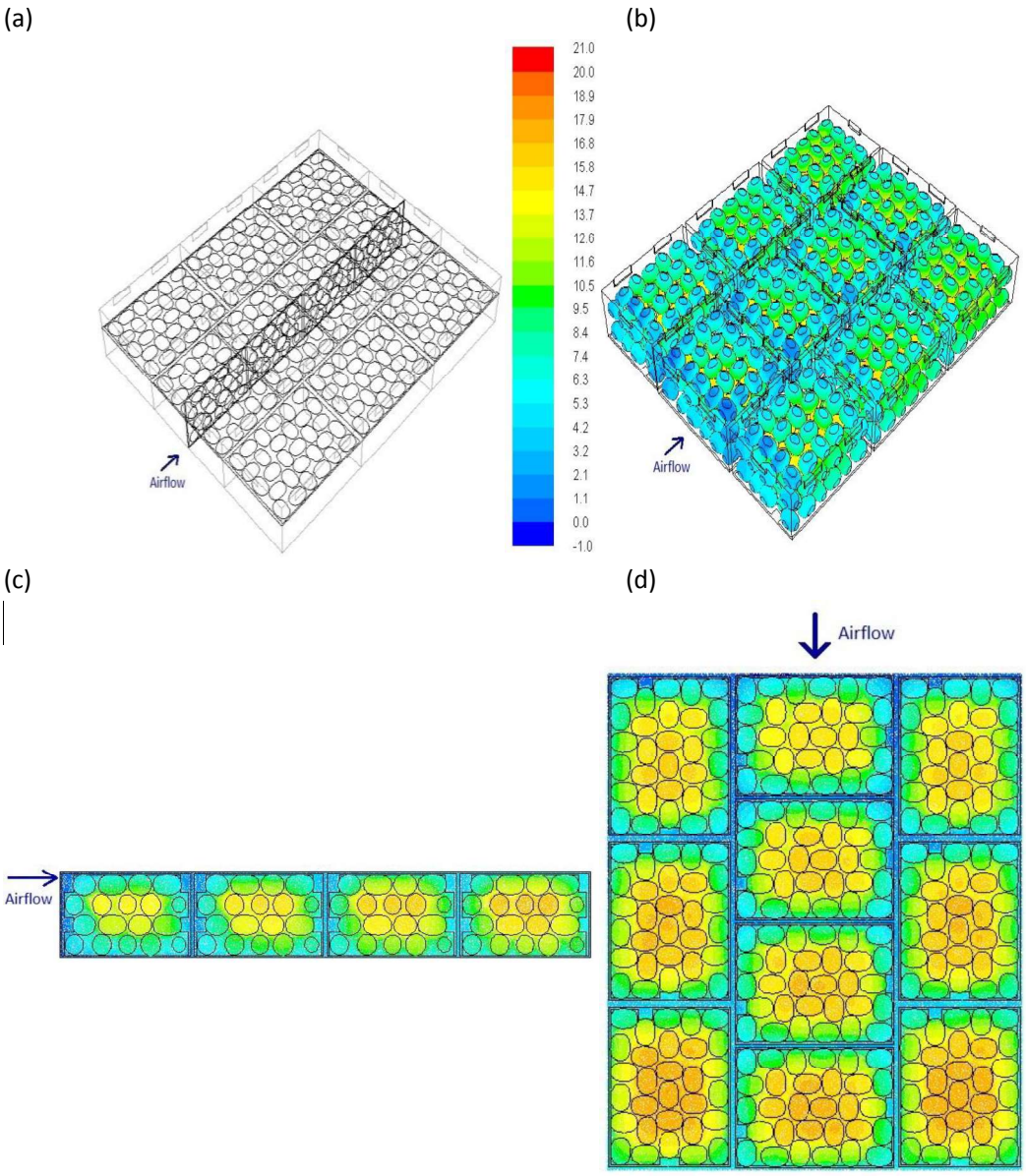

Figure 7. (a) Location of vertical and horizontal cross-sectional area through the pallet layer. Temperature distribution (°C) for (b) an isometric view of the kiwifruit temperature in each MBP, along the (c) vertical and (d) horizontal cross-sectional area, after 4.28 h (average pallet layer HCT) of forced air cooling for a pressure drop of 200 Pa (0.34 L kg^{-1} s^{-1}).

Figure 8

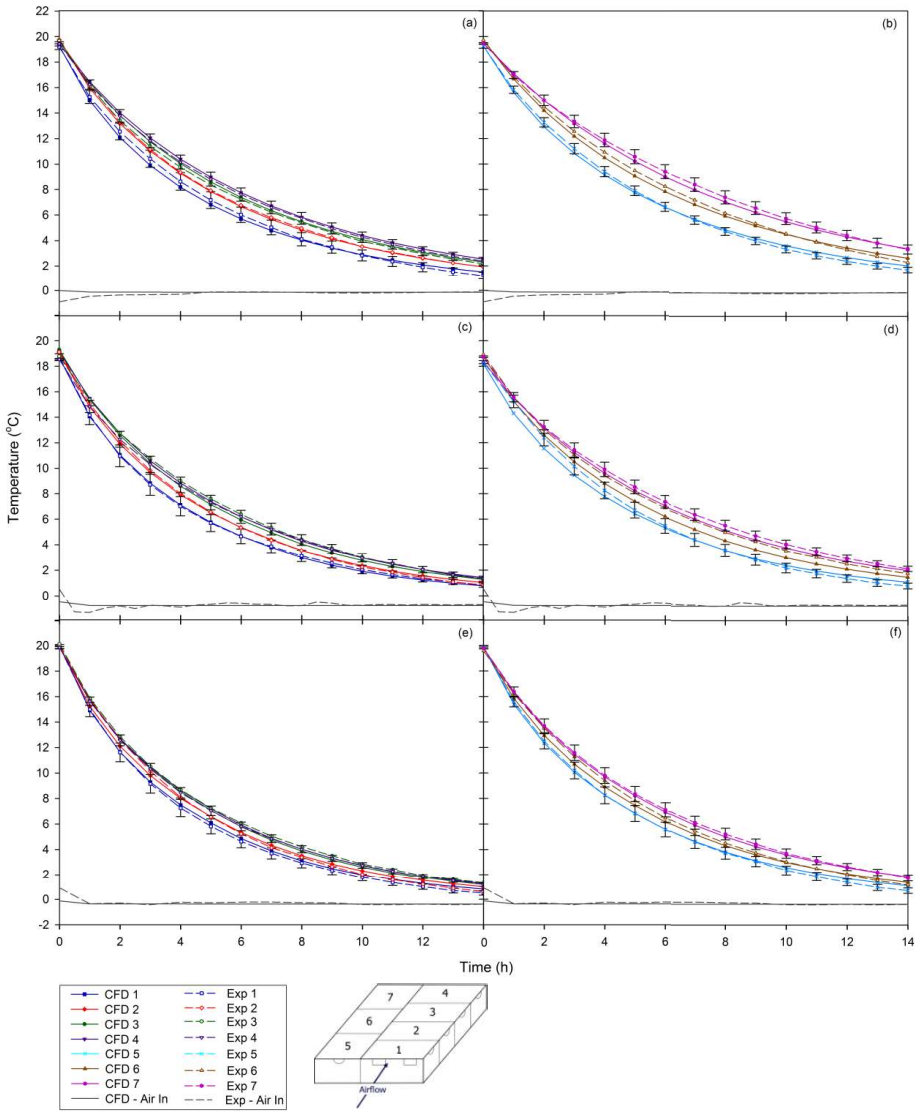

Figure 8. Comparison between predicted and experimental numerical average temperatures, during 14 h of forced-air cooling from an approximate initial product temperature of 20 °C, for (a) MBPs 1 - 4 at 0.34 L kg^{-1} s^{-1}, (b) MBPs 5 - 7 at 0.34 L kg^{-1} s^{-1}, (c) MBPs 1 - 4 at 0.51 L kg^{-1} s^{-1}, (d) MBPs 5 - 7 at 0.51 L kg^{-1} s^{-1}, (e) MBPs 1 - 4 at 0.71 L kg^{-1} s^{-1} and (f) MBPs 5 - 7 at 0.71 L kg^{-1} s^{-1}. Standard error bars are shown for MBPs 1, 4, 5 and 7. Experimental and predicted air temperatures, averaged between the inlet vents of MBPs 1 and 5, are also shown.

Figure 9

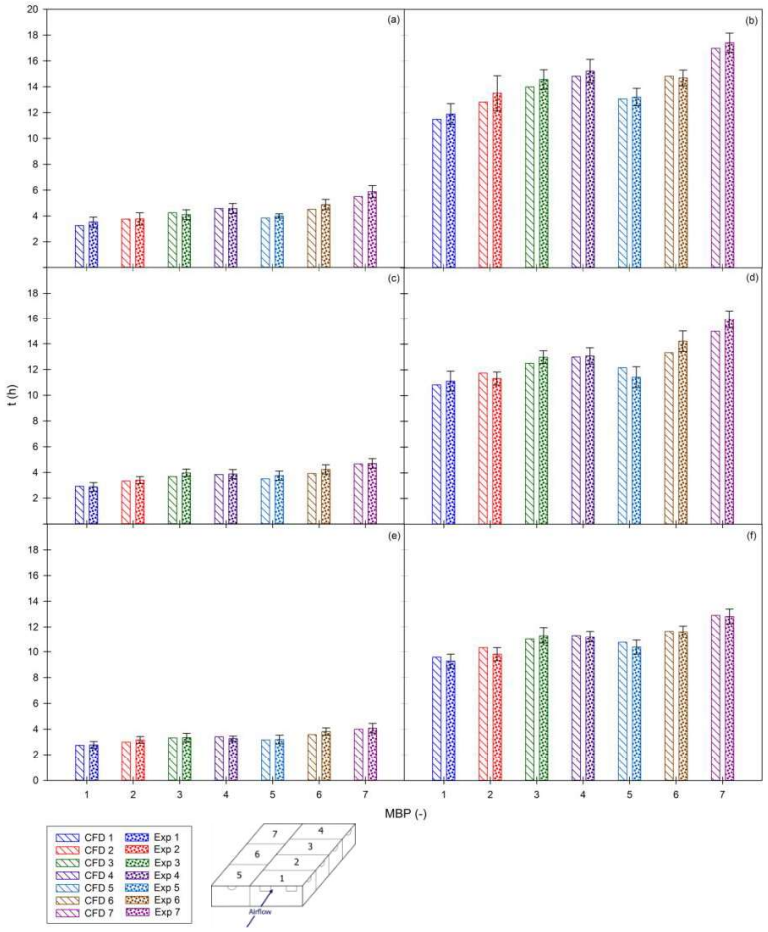

Figure 9. Predicted and experimental cooling times for MBPs 1 – 7 for (a) HCT at 0.34 L kg^{-1} s^{-1}, (b) SECT at 0.34 L kg^{-1} s^{-1}, (c) HCT at 0.51 L kg^{-1} s^{-1}, (d) SECT at 0.51 L kg^{-1} s^{-1}, (e) HCT at 0.71 L kg^{-1} s^{-1} and (f) SECT at 0.71 L kg^{-1} s^{-1}. Standard error bars are shown for each MBP.

Nomenclature

English Symbols

C_p – specific heat at constant pressure, J kg^{-1} K^{-1}
E – energy per unit mass, J kg^{-1}
h – specific enthalpy, J kg^{-1}
k – thermal conductivity, W m^{-1} K^{-1}
m – mass, kg
p – pressure, Pa
P – power, W
Q – volumetric flowrate, m^3 s^{-1}
t – time, s
T – temperature, K
v – velocity, m s^{-1}
$\vec{v}$ – overall velocity vector, m s^{-1}
x, y, z – Cartesian coordinates, m
Y – Fractional Unaccomplished Temperature Change, dimensionless

Greek Symbols

ε – turbulent dissipation rate, m^2 s^{-3}
κ – turbulent kinetic energy, m^2 s^{-2}
ρ – density, kg m^{-3}

Subscripts

a – air
avg – average
i – initial
t – turbulent
eff – effective

Abbreviations

CFD – Computational Fluid Dynamics
FUTC – Fractional Unaccomplished Temperature Change, -
HCT – Half Cooling Time, h
MBP – Modular Bulk Pack
RH – Relative Humidity, %

SECT – Seven Eights Cooling Time, h
TCR – Temperature Control Room
VSD – Variable Speed Drive

Tables

Table 1

Table 1. Material properties of the air and solid materials used in the numerical model.

	Material		
Properties	**Air (°C)**	**Kiwifruit**	**Cardboard**
Density (kg m^{-3})	1.293	1037	960
Specific heat capacity (J kg^{-1} K^{-1})	1006	3713	2300
Thermal conductivity (W m^{-1} K^{-1})	0.02343	0.542	0.48
Viscosity (kg m^{-1} s^{-1})	1.73×10^{-5}	–	–
Expansion coefficient (K^{-1})	0.00367	–	–

Table 2

Table 2. HCT, and the relative reduction in HCT, between the tested pressure drops/air flowrates for MBPs 1 – 7 in a pallet layer

			HCT (h)							
Δp (Pa)	**Q (L kg^{-1} s^{-1})**	**P (W)**	**MBP 1**	**MBP 2**	**MBP 3**	**MBP 4**	**MBP 5**	**MBP 6**	**MBP 7**	**Pallet $layer_{avg}$**
25	0.12	3.0	4.35	5.62	7.05	8.12	5.38	7.47	10.05	6.85
50	0.18	9.0	3.9	4.85	5.72	6.42	4.75	6.13	7.87	5.68
100	0.25	25.0	3.54	4.22	4.88	5.33	4.23	5.27	6.47	4.92
200	0.34	68.0	3.23	3.72	4.18	4.47	3.87	4.57	5.42	4.28
400	0.50	200.0	2.98	3.33	3.63	3.82	3.53	3.98	4.6	3.77
800	0.69	552.0	2.78	3.05	3.28	3.4	3.27	3.62	4.07	3.42
			Relative reduction in HCT (%) between pressure drop increases							
25	0.12	3.0	–	–	–	–	–	–	–	–
50	0.18	9.0	10.3	13.7	18.9	20.9	11.7	17.9	21.7	17.1
100	0.25	25.0	9.2	13.0	14.7	17.0	10.9	14.0	17.8	13.4
200	0.34	68.0	8.8	11.8	14.3	16.1	8.5	13.3	16.2	13.0
400	0.50	200.0	7.7	10.5	13.2	14.5	8.8	12.9	15.1	11.9
800	0.70	552.0	6.7	8.4	9.6	11.0	7.4	9.0	11.5	9.3